RSC Advances

Highly efficient Ni-Co oxide nanoparticles on nitrogen-doped FDU-15 for aerobic benzyl alcohol oxidation

Journal:	*RSC Advances*
Manuscript ID	RA-ART-04-2016-009756.R2
Article Type:	Paper
Date Submitted by the Author:	08-Jun-2016
Complete List of Authors:	Fu, Xiaoran; Jilin University, College of Chemistry Wu, Shujie; Jilin University, College of Chemistry li, Zhifang; Jilin University, College of Chemistry Yang, Xiaoyuan; Jilin University, College of Chemistry Wang, Xiufang; Jilin University, College of Chemistry Peng, Ling; Jilin University, College of Chemistry Hu, Jing; Jilin University, State Key Laboratory of Inorganic Synthesis and Preparative Chemistry, College of Chemistry, Huo, Qisheng; Jilin University, Chemistry Guan, Jingqi; Jilin University, College of Chemistry Kan, Qiubin; Jilin University, College of Chemistry
Subject area & keyword:	Heterogeneous < Catalysis

Journal Name

ARTICLE

Highly efficient Ni-Co oxide nanoparticles on nitrogen-doped FDU-15 for aerobic benzyl alcohol oxidation

Received 00th January 20xx,
Accepted 00th January 20xx

DOI: 10.1039/x0xx00000x

www.rsc.org/

Xiaoran Fu,[a] Shujie Wu,[a] Zhifang Li,[a] Xiaoyuan Yang,[a] Xiufang Wang,[a] Ling Peng,[a] Jing Hu,[a] Qisheng Huo,[b] Jingqi Guan*[a] and Qiubin Kan*[a]

Ni-Co bimetallic oxide catalysts with various loadings and Ni/Co ratios supported on N-doped FDU-15 were prepared by a facile and controllable one-pot method and tested as heterogeneous catalysts for the oxidation of benzyl alcohol. The prepared materials were characterized by a series of characterization techniques such as XRD, TEM, SEM-EDX, FT-IR, XPS, N_2 adsorption-desorption, Raman and ICP-AES. Catalytic results showed that 2 wt.% Ni-Co_3/FDU-15$_{-N}$ possessed very high substrate conversion (93.4%) and excellent benzaldehyde selectivity (97.8%) when using air as the oxidant at 110 ^{o}C. This superior catalytic performance over bimetallic catalysts indicated a synergy effect between Ni and Co. The improved redox ability and dispersion of Ni-Co alloying sites also contributed to this enhancement. Additionally, N-doped Ni-Co_3/FDU-15$_{-N}$ might strengthen the interaction between NiO, Co_3O_4 and the support and thus improve the dispersion of the metal oxides.

Introduction

The catalytic oxidation of benzyl alcohol is vitally important in modern chemical industry because the obtained benzaldehyde is an indispensable intermediate in the synthesis of fine chemicals and pharmaceuticals.[1,2] Traditionally, homogeneous catalytic systems (e.g. chiral metalloporphyrins, and metal-salen complexes) or hazardous stoichiometric oxidants (e.g. organic peracids, PHIO, or TBHP) have been employed to accomplish the benzyl alcohol oxidation reaction.[3,4] These procedures have considerable drawbacks, such as difficulty in catalyst separation and regenerability, utilization of unsafe and expensive oxidants resulting in serious environmental pollution and industrial loss of interest. With the ever-increasing economic and environmental concerns, the development of heterogeneous catalytic system that can operate with molecular oxygen in place of hazardous oxidants has drawn tremendous interest.[5-7]

For conventional heterogeneous catalysis, bimetallic catalysts often showed tunable and synergistic effects compared to their monometallic counterparts.[8-10] In particular, the synergistic catalysis of Au-based bimetallic nanocatalysts has received considerable interest along with the "gold rush".[11-14] For example, Hamill[13] et al. found that the combination of gold with palladium has a synergistic effect, showing higher catalytic activity for NO_x conversion than the corresponding mono-metallic materials. Among the non-noble metals, nickel and cobalt have been considered the best replacements for noble metals due to their large storage and low cost.[15-18] Wang and co-workers[18] reported amorphous Ni-Co catalyst for the hydrazine oxidation. As stated in many previous papers, factors as the interaction of the Ni-based materials with other metals or the support strongly determine the catalytic performances of these catalysts.[19,20] Gonzalez-delaCruz's group[19] reported the catalyst of Ni-Co oxide supported on ZrO_2 showed a better activity and stability than the nickel monometallic system in the dry reforming reaction of methane. Even though the cobalt monometallic system has no activity for the methane reforming reaction, the presence of adjacent nickel atoms seems to prevent the deposition of carbon over the cobalt sites, thus showing higher activity in the dry reforming reaction. This synergic effect accounts for the better performance of the bimetallic systems and points at both, as important factors responsible for the difference in catalytic activities and stabilities in alcohol oxidation reactions[21] and other oxidation reduction reactions.[22]

Mesoporous carbon material FDU-15 has received considerable attention owing to large surface area, tunable pore structure, uniform and adjustable pore size, chemically inert nature, mechanical stability, and good conductivity.[23-26] These outstanding features make it ideal candidate for applications in adsorption and separation,[23] catalysis,[24] electrochemistry,[25] and sensors[26]. However, FDU-15 has highly hydrophobic surface and a limited number of specific active sites, which impedes its practical application. Therefore, nitrogen is usually introduced into the carbon lattice to not only overcome these drawbacks, but also enhance mechanical and electrical properties of carbon materials.[27,28] Furthermore, N-doped FDU-15 not only can maintain the large specific

[a] Address, College of Chemistry, Jilin University, Changchun, 130023, P.R. China.
[b] Address, State Key Laboratory of Inorganic Synthesis and Preparative Chemistry, College of Chemistry, Jilin University, Changchun 130012, P.R. China.
[c] E-mail: guanjq@jlu.edu.cn (J.Q. Guan), qkan@mail.jlu.edu.cn (Q. Kan)

surface area, but also can improve metal dispersion and strengthen metal-support interaction.[29]

In the present work, we synthesize a novel recyclable heterogeneous catalyst Ni-Co_3/FDU-15$_{-N}$ by a one-pot controllable method for the oxidation of benzyl alcohol. The influence of catalyst amount, molar ratios of oxidant to benzyl alcohol, reaction temperature and time on catalytic performance has also been investigated.

Experimental

Material

Pluronic P123 ($EO_{20}PO_{70}EO_{20}$) was purchased from Aldrich. Hexadecane, $Co(NO_3)_2{\cdot}6H_2O$, $Ni(NO_3)_2{\cdot}6H_2O$, benzyl alcohol, toluene, concentrated ammonia aqueous solution (28 wt.%), formaldehyde (37%), ethanol (99.5%), N,N-dimethylformamide (DMF, 99.9%), acetonitrile (99.8%), $NH_3{\cdot}H_2O$ (28 wt.%) were used for synthesis. All the organic solvents were of analytical grade.

Synthetic procedures

The two dimensional hexagonal mesoporous carbon, FDU-15, was synthesized according to the literature.[30] As-synthesized FDU-15 was calcined at 800 ^{o}C for 3 h under nitrogen atmosphere. In a typical synthesis of Ni-Co_3/FDU-15$_{-N}$ catalysts, 0.125 g of FDU-15 was dispersed in 378 mL of ethanol by ultrasonic treatment. $Co(NO_3)_2{\cdot}6H_2O$ (0.033 mmol) and $Ni(NO_3)_2{\cdot}6H_2O$ (0.011 mmol) were completely dissolved into 0.23 mL of the water, which was then added into the above FDU-15 system, followed by addition of 0.095 mL $NH_3{\cdot}H_2O$ (28 wt.%) and 0.19 mL of water at room temperature. The reaction mixture was kept at 80 ^{o}C with stirring for 10 h. Then, the suspension was transferred into an autoclave, sealed and maintained at 150 ^{o}C for 3 h. Finally, the products were separated by centrifuging, washed with pure water, and then dried at 60 ^{o}C for 8 h. Three different Co/Ni molar ratio catalysts (Co/Ni = 1, 2, and 3) were synthesized, which was labeled as Ni-Co/FDU-15$_{-N}$, Ni-Co_2/FDU-15$_{-N}$, and Ni-Co_3/FDU-15$_{-N}$, respectively.

For comparison, Co/FDU-15$_{-N}$ and Ni/FDU-15$_{-N}$ were also prepared by the similar method. Ni-Co_3/FDU-15 was prepared by using sodium hydroxide to replace ammonium hydroxide in the synthetic route.

Characterization

Small angle powder XRD patterns were collected with a Riguku D/MAX2550 diffractometer with Cu-Kα radiation at 50 kV and 200 mA. The diffractions were recorded in the 2θ range of 0.6-5^{o} and in steps of 1^{o}/min. The morphologies of the nanocomposites were obtained using a JEOL JEM-2010 transmission electron microscope (TEM). The infrared spectra of the materials were conducted on a Nicolet 6700 instrument in the range of 400-4000 cm^{-1} using KBr pellet technique. The N_2 adsorption-desorption isotherms were recorded at -196 ^{o}C on an adsorption analyzer (Micro-meritics ASAP 2010). Prior to this measurement, each sample was degassed at 120 ^{o}C for 5 h. The specific surface area was determined using the Brunauer-Emmett-Teller (BET) equation and pore size distribution was calculated using Barrett-Joyner-Halenda (BJH) algorithm. X-ray photoelectron spectroscopy (XPS) was measured on Scienta ESCA200 spectrometer using Al-Kα radiation. Raman spectra were recorded on a Renishaw Raman system model 1000 spectrometer with an excitation wavelength of 514 nm. The metal content of the catalysts was measured by inductively coupled plasma atomic emission analysis (ICP-AES, Perkin-Elmer Optima 3300 DV).

Results and discussion

Structural integrity studies

Fig. 1a shows the small-angle XRD pattern of the FDU-15, in which the strong (100) diffraction peak at 0.6-1.5^{o} of 2θ can be observed, illustrating that the FDU-15 has a mesostructure.[31,32] After loading Ni-Co NPs onto the FDU-15, no significant spectral feature changes were observed, indicating that the ordered mesoporous structure remained unchanged after the incorporation of Ni-Co nanoparticles.[33] Furthermore, the intensity of the peaks (Fig. 1b) has decreased to a certain extent, while the full width at half-maximum of the peaks that is normalized by height has increased. In addition, no clear peaks assignable to Ni, Co species were observed in the XRD pattern (Figure. 2e).

The internal morphology of the support and the bimetallic catalysts were studied by TEM (Fig. 3). As shown in Fig. 3a, the pristine FDU-15 shows highly ordered stripe-like, which is in agreement with the result of low-angle XRD.[31,34] Compared with the catalyst Ni-Co_3/FDU-15 without nitrogen doped treatment (Fig.3c), the small Ni-Co NPs (dark spots) of the Ni-Co_3/FDU-15$_{-N}$ catalyst are better dispersed (Fig. 3b) [29]. SEM analysis revealed that Co and Ni nanoparticles were formed on FDU-15 (Fig. 4), and in the corresponding elemental maps (C, O, N, Co, and Ni) obtained by energy dispersive X-ray EDX analysis (Fig. 4), Co and Ni atoms were found to be uniformly dispersed on the FDU-15. Combining with the above TEM results, it can be inferred that the NiO and Co_3O_4 should be mainly presented as mixed oxide, while some heterostructure between NiO and Co_3O_4 cannot be excluded.

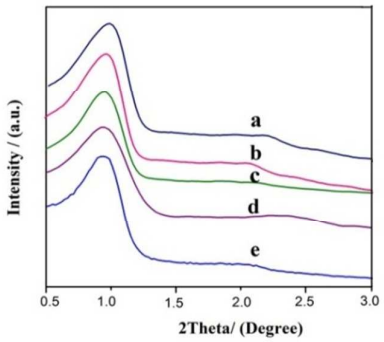

Fig. 1. Small-angle XRD patterns of (a) FDU-15, (b) Co/FDU-15$_{-N}$, (c) Ni/FDU-15$_{-N}$ (d) Ni-Co_3/FDU-15 and (e) Ni-Co_3/FDU-15$_{-N}$.

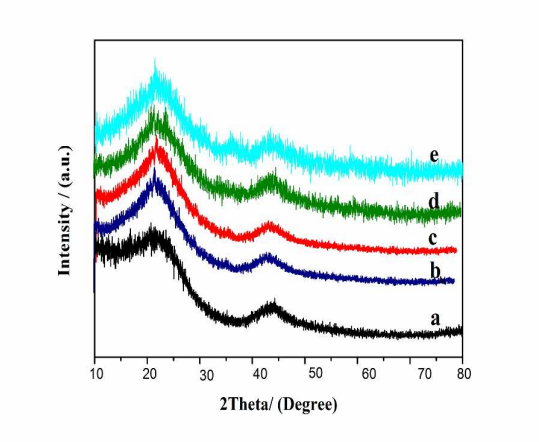

Fig.2. Wide-angle XRD patterns of (a) FDU-15, and (b) Co/FDU-15$_{-N}$, (c) Ni/FDU-15$_{-N}$ (d) Ni-Co_3/FDU-15 and (e) Ni-Co_3/FDU-15$_{-N}$.

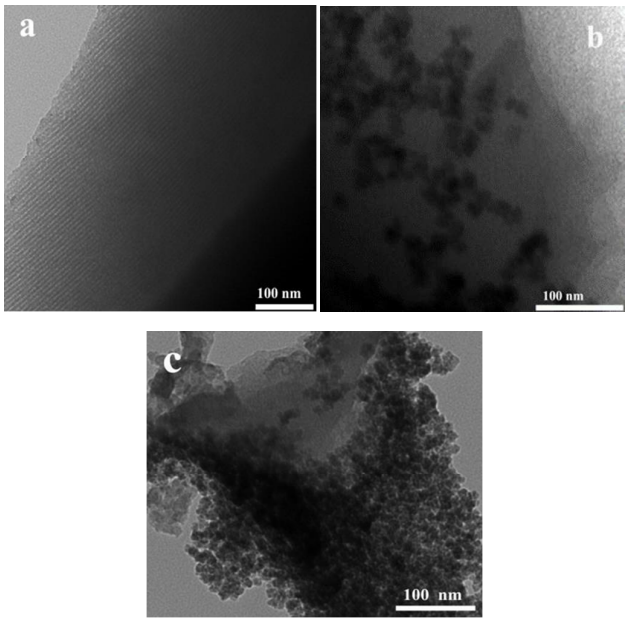

Fig. 3. TEM images of (a) FDU-15, (b) Ni-Co_3/FDU-15$_{-N}$, (c) Ni-Co_3/FDU-15.

The nitrogen adsorption-desorption isotherms of FDU-15 and Ni-Co_3/FDU-15$_{-N}$ are shown in Fig. 5. The adsorption and desorption branches of FDU-15 are not close at low relative pressure, suggesting a typical sorption behavior of polymer materials.[30,35] The first stage at P/P_0 < 0.4 is due to a monolayer adsorption of nitrogen molecules on the walls of the mesopores. The second stage, at 0.4< P/P_0 < 0.8, is characterized by a steep increase in adsorption due to capillary condensation inside the mesopores. The third stage is a tail portion at P/P_0 > 0.8, associated with multilayer adsorption on the external surface of the materials. In comparison to the parent FDU-15, Ni-Co_3/FDU-15$_{-N}$ exhibits a decreased uptake of nitrogen, owing to the immobilization of Ni-Co NPs. Table 1 summarizes the nitrogen sorption results. The Brunauer-

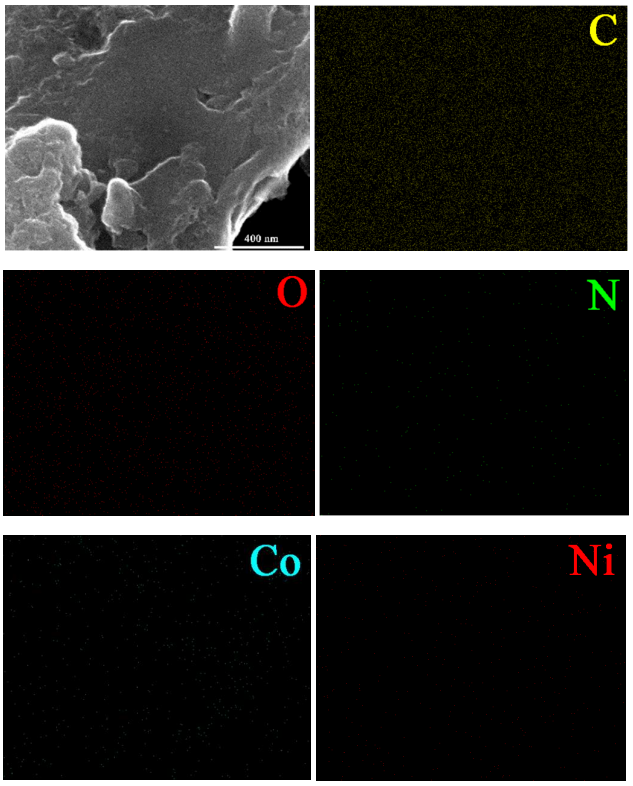

Fig. 4. SEM image of Ni-Co_3/FDU-15$_{-N}$ and corresponding EDX maps of C, O, N, Co, and Ni, respectively.

Emmett-Teller (BET) surface area of FDU-15 is 907 $m^2 \cdot g^{-1}$ with pore volume of 0.45 $cm^3 \cdot g^{-1}$ in agreement with those reported data. Ni-Co_3/FDU-15$_{-N}$ shows less nitrogen uptake (BET surface area of 756 $m^2 \cdot g^{-1}$ and pore volume of 0.35 $cm^3 \cdot g^{-1}$).

Spectroscopic characterization

The FT-IR spectra of FDU-15 and Ni-Co_3/FDU-15$_{-N}$ are shown in Fig. 6. For FDU-15, the peaks at 1727 and 1741 cm^{-1} can be assigned to the C=O stretching vibrations due to auto-oxidation process of the methylene bridges, while the peak at 3334 cm^{-1} can be assigned to the phenolic -OH stretching vibrations. For Ni-Co_3/FDU-15$_{-N}$, the less resolved additional band centered at 673 cm^{-1} is attributed to the stretching vibrations of Co=O bond. The stretching vibrations of Ni=O bands are at approximately 404, 464 and 501 cm^{-1}.[36,37]

Raman spectra of FDU-15, Co/FDU-15-N and Ni-Co_3/FDU-15$_{-N}$ are shown in Fig.7. The peak at 1580 cm^{-1} (G band) is attributed to the vibration of sp^2-bonded carbon atoms in a two-dimensional hexagonal lattice, namely the stretching modes of C=C bonds typical of graphite, while the peak at 1350 cm^{-1} (D band) is associated with vibrations of carbon atoms with dangling bonds of plane terminations of disordered graphite and related to the defects and disorders in structures in carbon materials.[38] The relative intensities of these two bands depend on the type of graphitic material and reflect the graphitization degree. The calculated I(D)/I(G) relative intensity ratios of FDU-15, Co/FDU-15 and Ni-Co_3/FDU-15$_{-N}$ are 2.2, 2.5, and 2.8, respectively. Compared with the I(D)/I(G) of

FDU-15, the I(D)/I(G) of the supported catalysts increase, which indicates that the size of the in-plane sp^2 domains decreases and the NiCo-based nanoparticles onto FDU-15 cause some defects or deoxygenation. In addition, the blue shift of G-band and D-band in Fig. 7b and 7c reveals that the bond energy between the NiCo-based nanoparticles and FDU-15 increases.

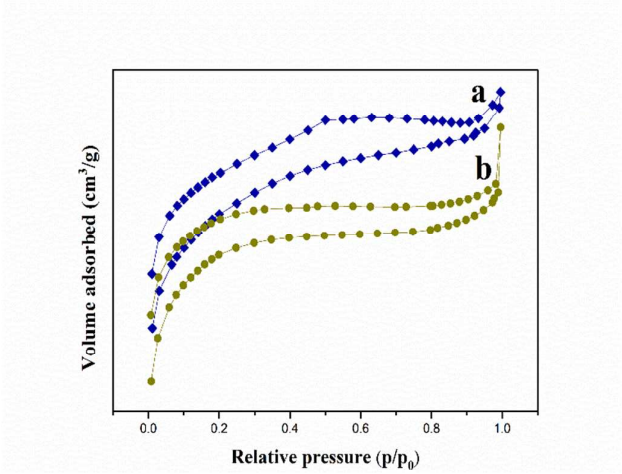

Fig. 5. N_2 adsorption-desorption isotherms of (a) FDU-15 and (b) Ni-Co_3/FDU-15$_{-N}$.

Table 1 Textural properties of samples.

Sample	S_{BET} (m^2 g^{-1})	V_{BJH} (cm^3 g^{-1})
FDU-15	907	0.45
Ni-Co_3/FDU-15$_{-N}$	756	0.35

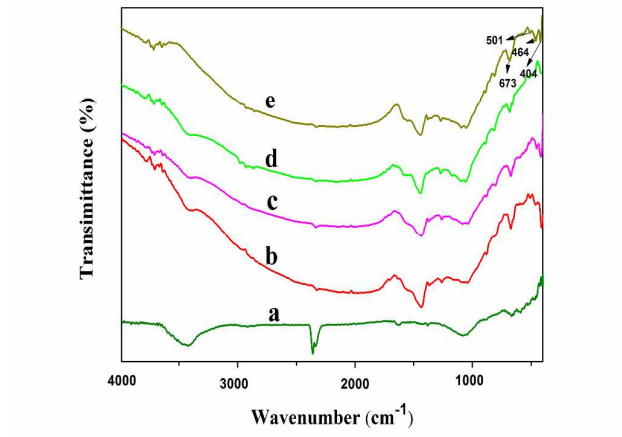

Fig. 6. FT-IR spectra of (a) FDU-15, (b) Co/FDU-15$_{-N}$, (c) Ni/FDU-15$_{-N}$ (d) Ni-Co_3/FDU-15 and (e) Ni-Co_3/FDU-15$_{-N}$.

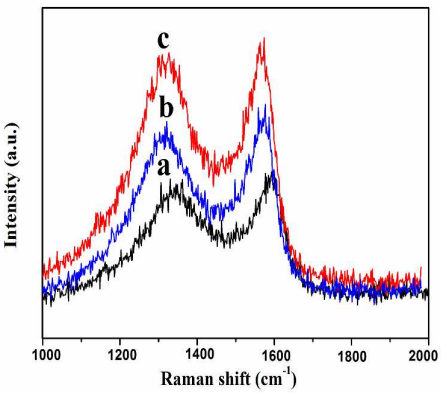

Fig. 7. Raman spectra of (a) FDU-15, (b) Co/FDU-15$_{-N}$, and (c) Ni-Co_3/FDU-15$_{-N}$

XPS studies

To determine the electronic state and the composition of the Ni-Co_3/FDU-15$_{-N}$ composites, the XPS measurements were carried out (Fig. 8). As shown in the XPS survey scan spectrum (Fig. 8a), Ni-Co_3/FDU-15$_{-N}$ was primarily composed of Ni 2p, Co 2p, C 1s, O 1s and N 1s peaks, signifying the presence of Ni, Co, C, O and N elements in the sample. Fig. 8b and c show the high-resolution XPS spectra of Co 2p and Ni 2p of the Ni-Co_3/FDU-15$_{-N}$. Two spectral curves commonly exhibited the spin-orbit splitting into $2p_{1/2}$ and $2p_{3/2}$ with shake-up satellites (indicated by 'Sat'). For the high-resolution spectra of Co 2p, the binding energy values of 780.9 and 796.4 eV were observed for the Co $2p_{1/2}$ and Co $2p_{3/2}$ regions, which correspond to the Co^{2+} valence state of cobalt hydroxide as shown in Fig. 8b. Meanwhile, in the Ni 2p curve of Fig. 8c, the binding energy values of 873.5 and 855.7 eV correspond to the Ni $2p_{1/2}$ and Ni $2p_{3/2}$ with spin-orbit characteristics of Ni^{2+} in nickel hydroxide. Compared with the reported Ni and Co binding energy values [39,40], these values in Ni-Co_3/FDU-15$_{-N}$ are slightly shifted towards lower values, which could indicate the synergistic effect of Co-Ni. In addition, the high-resolution N 1s spectrum of Ni-Co_3/FDU-15$_{-N}$ (Fig. 8d) reveals the presence of pyrrolic (400.2 eV) N atoms.[41]

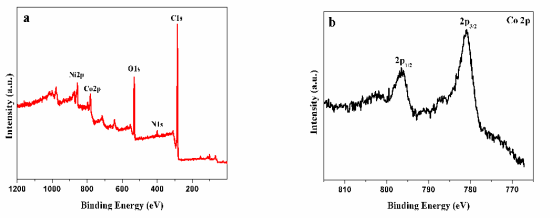

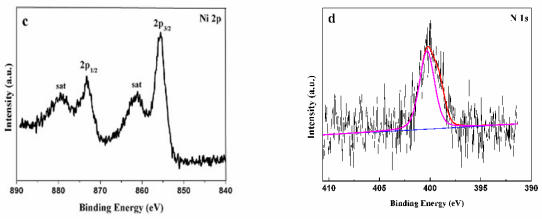

Fig. 8. XPS survey spectrum of Ni-Co_3/FDU-15_{-N} (a), and detailed spectrum of Co2p (b), Ni2p (c), and N1s (d).

Catalytic properties

The catalytic performance of Ni-Co_3/FDU-15_{-N} was carried out in the benzyl alcohol oxidation with air as oxidant. In order to get the optimal reaction conditions, different parameters such as molar ratio of metal, solvent, reaction time, and temperature were investigated.

From the results of different Ni/Co molar ratios in Table 2, it can be seen that the conversion of benzyl alcohol remarkably improves from 60.6% to 93.4% after 7 h by decreasing the Ni/Co molar ratio from 1:1 to 1:3. It is also found that the benzaldehyde selectivity also increases by lessening the Ni/Co molar ration. The co-doping of Ni-Co can significantly improve the surface coverage of the redox species, as well as adjust the benzyl alcohol adsorption.[42] We have also performed the oxidation of benzyl alcohol in different solvents, such as DMF, acetonitrile, water, ethanol and toluene. Toluene is a non-polar solvent, while acetonitrile, water ethanol and DMF are polar solvents. From Table 2, toluene, water ethanol and acetonitrile are not the desired solvents, in which just 1.2% ~ 67.5% conversion are obtained after 7 h reaction. However, when DMF is used as the solvent for the reaction, the conversation of benzyl alcohol could reach as high as 93.4% after 7 h. The influence of the reaction temperature on the catalytic reaction is also investigated as listed in Table 2. The conversion decreased to 86.1% with the decrease in the temperature to 100 ^{o}C. In the meantime, the conversion slightly increases when the reaction temperature rises to 120 ^{o}C, while the selectivity to benzaldehyde obviously decreases. Considering the above information, the optimal reaction temperature should be 110 ^{o}C.

Compared with a series of heterogeneous catalyst conducted by previous reports (Table 3), it is obvious that Ni-Co_3/FDU-15_{-N} possesses the highest conversation, benzaldehyde selectivity and turnover frequency. Most importantly, it should be noted that the combination of other congeneric metals has not so good catalytic performance (Table 3, entries 7-11). For example, only 39.5% conversion of benzyl alcohol and 89.2% selectivity to benzaldehyde can be obtained over Co_2MgAl-LDH. In addition, the excellent catalytic performance of Ni-Co_3/FDU-15_{-N} can attribute to the N-doped mesoporous structures to avoid pore blockage and facilitate reactants diffusion into the pores (Table 3, entries 1-4). Moreover, the conversion of benzyl alcohol achieves a superior value at 7 h and the average TOF value reaches 19.5 h^{-1}. This result also means that the synergistic effect between Ni-Co NPs and N-doped FDU-15 support is superior to the others.

The stability and reusability of Ni-Co_3/FDU-15_{-N} are of great importance in terms of practical application and green chemistry. After each reaction, the catalyst was collected using a filtration, washed thoroughly, dried under vacuum and reused for the subsequent cycles. In a series of 4 consecutive runs, Ni-Co_3/FDU-15_{-N} exhibits basically stable catalytic activity and selectivity (i.e. conversion: 93.4-91.8%, selectivity: 97.8-96.5%) (Fig. 9). In order to further evaluate the stability of Ni-Co_3/FDU-15_{-N} during the catalytic process, the leaching test was carried out and the results are shown in Fig. 10. The aerobic reaction was suspended after 2 hours. Subsequently, the catalyst was underwent filtration separation under hot conditions, and the resulting clear solution was stirred for another 5h at 110 ^{o}C. Nevertheless, no obvious improvement in benzyl alcohol conversion can be observed after the Ni-Co_3/FDU-15_{-N} catalyst was removed. After completion of the reaction, the solution was subjected to inductively coupled plasma analysis techniques; almost no detectable nickel, cobalt metal ions in the filtrate solution. These results indicate that the Co_3/FDU-15_{-N} catalyst is rather stable in the catalytic process because almost no metal leaching happens.

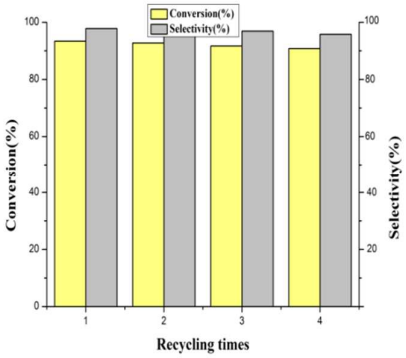

Fig. 9. Reuse of the Ni-Co_3/FDU-15_{-N} catalyst.

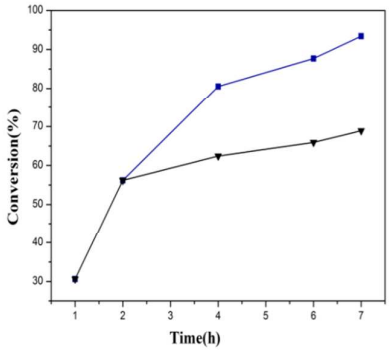

Fig. 10. Leaching experiments of Ni-Co_3/FDU-15_{-N} for aerobic oxidation of benzyl alcohol.

Journal Name

ARTICLE

Table 2 Benzyl alcohol oxidation under various reaction conditions [a]

Entry	Catalyst	Solvent	Time (h)	Temperature (°C)	Conversion (%)	Product selectivity (%)	
						Benzaldehyde	Others
1	Ni-Co_3/FDU-15$_{-N}$	DMF	7	110	93.4	97.8	2.2
2	Ni-Co_2/FDU-15$_{-N}$	DMF	7	110	75.7	83.4	16.6
3	Ni-Co/FDU-15$_{-N}$	DMF	7	110	60.6	79.5	10.2
4	Ni-Co_3/FDU-15$_{-N}$	DMF	7	120	95.7	93.6	5.4
5	Ni-Co_3/FDU-15$_{-N}$	DMF	7	100	86.1	95.3	4.7
6	Ni-Co_3/FDU-15$_{-N}$	CH_3CN	7	110	16.7	>99	-
7	Ni-Co_3/FDU-15$_{-N}$	Water	7	110	1.2	>99	-
8	Ni-Co_3/FDU-15$_{-N}$	Toluene	7	110	12.7	>99	-
9	Ni-Co_3/FDU-15$_{-N}$	Ethanol	7	110	67.5	99.3	0.7
10	Ni-Co_3/FDU-15$_{-N}$	DMF	6	110	87.7	94.4	7.6
11	Ni-Co_3/FDU-15$_{-N}$	DMF	5	110	82.5	93.1	6.9
12	Ni-Co_3/FDU-15$_{-N}$	DMF	8	110	94.5	89.6	8.2

[a] Reaction condition: catalyst 50 mg, benzyl alcohol 1 mmol, DMF 10 ml, flow of air 80 ml/min.

Table 3 Comparison of various heterogeneous catalysts for aerobic oxidation of benzyl alcohol

Entry	Catalyst	Solvent	Oxidant	Time (h)	Conversion (%)	TOF (h^{-1})	Product selectivity (%)		Reference
							Benzaldehyde	Others	
1	Ni-Co_3/FDU-15$_{-N}$	DMF	Air	7	93.4	19.5	97.8	2.2	Herein
2	Ni-Co_3/FDU-15	DMF	Air	7	76.4	16.9	97.2	2.8	Herein
3	Ni/FDU-15$_{-N}$	DMF	Air	7	67.3	14.8	98.5	1.5	Herein
4	Co/FDU-15$_{-N}$	DMF	Air	7	87.9	17.7	89.1	10.9	Herein
5	No catalyst	DMF	Air	7	2	-	>99	-	Herein
6	FDU-15	DMF	Air	7	6.5	-	>99	-	Herein
7	NiAl-hydrotalcite	-	Air	9	47	-	98.5	1.5	42
8	Co-Ni ferrite	CH_3CN	TBHP	6	18.9	10.7	90.1	9.9	43
9	Co_2MgAl-LDH	CH_3CN	TBHP	12	39.5	9.6	89.2	10.8	44
10	Cu-CrHT	DMF	-	24	26	-	43	57	45
11	Co_3O_4/CMK-3	DMF	Air	6	82.1	12.5	97.7	2.3	35

Conclusions

Novel heterogeneous catalysts have been synthesized by covalently anchored transition bimetal (Ni, Co) oxide nanoparticles onto nitrogen-doped FDU-15. The characterization results demonstrated that transition metal oxides have been successfully incorporated onto nitrogen-doped FDU-15, while the pore structure of FDU-15 remained intact after multiple synthetic procedures. Compared with single NiO or Co_3O_4 NPs grafted onto N-doped FDU-15, Ni-Co co-doped Ni-Co_3/FDU-15$_{-N}$ exhibited better catalytic performance in the selective oxidation of benzyl alcohol with 93.4% conversion and 97.8% benzaldehyde selectivity. The excellent catalytic behaviour should be ascribed to the synergistic effect between NiO and Co_3O_4 NPs, large specific surface area and mesoporous structure of FDU-15 support, and N-dopant in the FDU-15 to improve the metal oxides dispersion and strengthen the interaction between metal oxides and the support. In addition, the heterogeneous Ni-Co_3/FDU-15$_{-N}$ was stable in the benzyl alcohol oxidation reaction, which can be reused four times without significant loss in the catalytic activity.

Acknowledgements

This work was supported by the National Natural Science Foundation of China (21303069) and Jilin province (20150520013JH).

Notes and references

1 D. I. Enache, J. K. Edwards, P. Landon, B. Solsona-Espriu, A. F. Carley, A. A. Herzing, M. Watanabe, C. J. Kiely, D. W. Knight, G. J. Hutchings, *Science*, 2006, **311**, 362.
2 P. Weerachawanasaka, G. J. Hutchingsb, J. K. Edwardsb, S. A. Kondratb, P. J. Miedziakb, P. Praserthama, J. Panpranota, *Catal. Today.*, 2015, **250**, 218.
3 D. Habibi, A. R. Faraji, *C. R. Chimie.*, 2013, **16**, 888.
4 Y. Zhu, M. Shen, Y. Xia, M. Lu, *Appl. Organometal. Chem.*, 2015, **29**, 152.
5 S. Sarina, H. Zhu, E. Jaatinen, Q. Xiao, H. Liu, J. Jia, C. Chen, J. Zhao, *J. Am. Chem. Soc.*, 2013, **135**, 5793.
6 A. Villa, D. Wang, D. Sucd, L. Prati, *Catal. Sci. Technol.*, 2015, **5**, 55.
7 Q. He, P. J. Miedziak, L. Kesavan, N. Dimitratos, M. Sankar, J. A. Lopez-Sanchez, M. M. Forde, J. K. Edwards, D. W. Knight, S. H. Taylor, C. J. Kiely, G. J. Hutchings, *Faraday Discuss.*, 2013, **162**, 365.
8 L. Jia, T. Zhou, J. Xu, X. Li, K. Dong, J. Huang, Z. Xu, *Nanoscale. Res. Lett.*, 2016, **11**, 1.
9 Y. Wei, Z. Zhao, B. Jin, X. Yu, J. Jiao, K. Li, J. Liu, *Catal. Today.*, 2015, **251**, 103.
10 S. Hamid, M, Kumar, W, Lee, *Appl. Catal. B-Environ.*, 2016, **187**, 37.
11 S. Wang, J. Wang, Q. Zhao, D. Li, J. Wang, M. Cho, H. Cho, O. Terasaki, S. Chen, Y. Wan, *Acs. Catal.*, 2015, **5**, 797.
12 T. Jiang, C. Jia, L. Zhang, S. He, Y. Sang, H. Li, Y. Li, X. Xu, H, Liu, *Nanoscale*, 2015, **7**, 209.
13 C. Hamill, R. Burcha, A. Gogueta, D. Rooneya, H. Drissb, L. Petrovb, M. Daousb, *Appl. Catal. B-Environ.*, 2014, **147**, 864.
14 W. Cui, Q. Xiao, S. Sarinac, W. Aoa, M. Xied, H. Zhuc, Z. Baoa, *Catal. Today.*, 2014, **235**, 152.
15 M. Zhao, T. L. Church, A. T. Harris, *Appl. Catal. B- Environm.*, 2011, **101**, 522.

16 C. R. B. Silva, L. Conceição, N. F. P. Ribeiro, M. M. V. M. Souza, *Catal. Commun.*, 2011, **12**, 665.
17 N. A. M. Barakata, M. Motlakc, *Appl. Catal. B-Environ.*, 2014, **154**, 221.
18 H. Wang, Y. Ma, R. Wang, J. Key, V. Linkovb, S. Ji, *RSC Adv.*, 2015, **51**, 3570.
19 V. M. Gonzalez-delaCruz, R. Pere˜ niguez, F. Ternero, J.. Holgado, A. Caballero, *J. Phys. Chem. C.*, 2012, **116**, 2919.
20 N. A.M. Barakata, M. Motlakc, B. Kima, A. G. El-Deend, S. S. Al-Deyabe, A.M. Hamzaf, *J. Mol. Catal. A-Chem.*, 2014, **394**, 177.
21 F. Liu, Y. Qu, Y. Yue, G. Liuab, Y. Liu, *RSC Adv.*, 2015, **5**,16837.
22 J. Zhang, H. Wang, A. K. Dalai, *J. Catal.*, 2007, **249**, 300.
23 M. Wang, X. Wang, Q. Yue, Y. Zhang, Ch. Wang, J. Chen, H. Cai, H. Lu, A. Elzatahry, D. Zhao, Y.Deng, *Chem. Mater.*, 2014, **26**, 3316.
24 H. Cai, L. Tian, B. Huang, G. Yang, D. Guan, H. Huang, *Micropor. Mesopor. Mat.*, 2013, **170**, 20.
25 D. Nie, Y. Liang, T. Zhou, X. Li, G. Shi, L. Jin, *Bioelectrochemistry*, 2010, **79**, 248.
26 K. Wang, H. Yang, L. Zhua, Z. Ma, S. Xing, Q. Lv, J. Liao, C. Liua, W. Xing, *Electrochim. Acta.*, 2009, **54**, 4626.
27 J. Wei, D. Zhou, Z. Sun, Y. Deng, Y. Xia, D. Zhao, *Adv. Funct. Mater.*, 2013, **23**, 2322.
28 J. Tang, T. Wang, X. Pan, X. Sun, X. Fan, Y. Guo, H. Xue, J. He, *J. Phys. Chem. C.*, 2013, **117**, 16896.
29 Z. Zhao, Y. Dai, G. Ge, Q. Mao, Z. Rong, G. Wang, *ChemCatChem*, 2015, **7**, 1070.
30 F. Zhang, Y. Meng, D. Gu, Y. Yan, Z. Chen, B. Tu, D. Zhao, *Chem. Mater.*, 2006, **18**, 5279.
31 Q. Xu, G. Xu, J. Yin,. A. Wang, Y. Ma, J. Gao, *Ind. Eng. Chem. Res.*, 2014, **53**, 10366.
32 B. Li, Y. Zhu, X. Jin, *J. Solid. State. Chem.*, 2015, **221**, 230.
33 X. Deng, W. Schmidt, H.Tuysuz, *Chem. Mater.*, 2014, **26**, 6127.
34 E. Kockrick, F. Schmidt, K. Gedrich, M. Rose, T. George, T. Freudenberg, R. Kraehnert, R. Skomski, D. J. Sellmyer, S. Kaskel, *Chem. Mater.*, 2010, **22**, 1624.
35 X. Yang, S. Wu, L. Peng, J. Hu, X. Wang, X. Fu, Q. Huob, J. Guan, *RSC Adv.*, 2015, **5**, 102508.
36 S. Bhunia, S. Jana, D. Saha, B. Dutta, S. Koner, *Catal. Sci. Technol.*, 2014, **4**, 1820.
37 R. Ramasamy, K. Ramachandran, G. Philip, R. Ramachandran, H. Therese, G. Gnana kumar, *RSC Adv.*, 2015, **5**, 76538.
38 R. Atchudan, S. Perumal, D. Karthikeyan, A. Pandurangan, Y. R. Lee, *Micropor. Mesopor. Mat.*, 2015, **215**, 123.
39 G. Nagaraju, G. S. R. Raju, Y. H. Ko, J. S. Yu, *Nanoscale*, 2016, **8**, 812.
40 X. Rong, F. Qiu, J. Qin, H. Zhao, J. Yan, D. Yang, *J. Ind. Eng. Chem.*, 2015, **26**, 354.
41 S. I. Tanase, D. Tanase, M. Dobromir, A. V. Sandu, V. Georgescu, *J. Supercond. Nov. Magn.*, 2016, **29**,469.
42 B.M. Choudary, M.L. Kantam, A. Rahman, C.V. Reddy, K.K. Rao, *Angew. Chem. Int. Edit.*, 2001, **40**, 763.
43 J. Tong, Q. Zhang, L. Bo, L. Su, Q. Wang, *J. Sol-Gel. Sci. Technol.*, 2015, **76**, 19.
44 W. Zhou, J. Liu, J. Pan, F. Sun, M. He, Q. Chen, *Catal. Commun.*, 2015, **69**, 1.
45 V. Choudhary, D. Dumbre, B. Uphade, V. Narkhede, *J. Mol. Catal. A-Chem.*, 2004, **215**, 129.

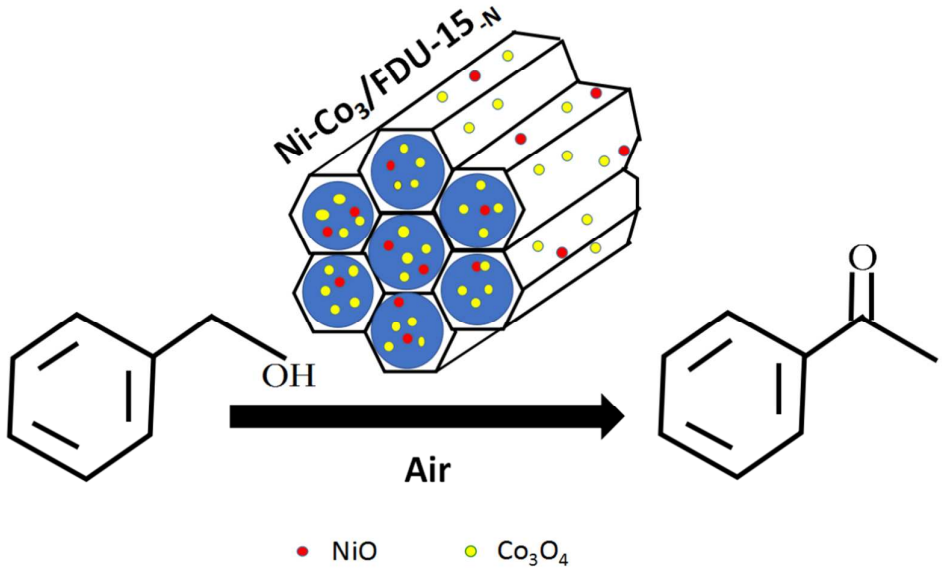

Transition bimetal (Ni, Co) oxide nanoparticles immobilized onto nitrogen-doped FDU-15 are high active and show excellent selectivity to the benzaldehyde for the oxidation of benzyl alcohol.